Postmodulation of the Metal–Organic Framework Precursor toward the Vacancy-Rich Cu x O Transducer for Sensitivity Boost: Synthesis, Catalysis, and H 2 O 2 Sensing

Serge Cosnier, Junji Li, Wen-Li Xin, Yu-Xuan Dai, Guofang Shu, Xue-Ji Zhang, Robert Marks, Dan Shan

Modulation of Crystalline Metal-organic Framework Precursor towards Carbon-based CuxO Electro-catalyst for Boosting Sensitive Hydrogen Peroxide Detection: Synthesis, Catalysis and Sensing Application

Journal:	*Analytical Chemistry*
Manuscript ID	ac-2021-021836
Manuscript Type:	Technical Note
Date Submitted by the Author:	24-May-2021
Complete List of Authors:	Li, Junji; Nanjing University of Science and Technology, School of Environmental & Biological Engineering Xin, Wen-Li; Nanjing University of Science and Technology Dai, Yu-Xuan; Nanjing University of Science and Technology, School of Environmental & Biological Engineering Shu, Guofang; Southeast University Zhongda Hospital Zhang, Xueji; Nanjing University of Science and Technology, School of Environmental & Biological Engineering Marks, Robert; Ben-Gurion University of the Negev, Department of Biotechnology Engineering Cosnier, Serge; Universite Grenoble Alpes, Département de Chimie Moléculaire UMR CNRS 5250 Shan, Dan; Nanjing University of Science and Technology, School of Environmental and Biological Engineering

Modulation of Crystalline Metal-organic Framework Precursor towards Carbon-based Cu_xO Electro-catalyst for Boosting Sensitive Hydrogen Peroxide Detection: Synthesis, Catalysis and Sensing Application

Junji Li[a], Wen-Li Xin[a], Yu-Xuan Dai[a], Guofang Shu[b], Xue-Ji Zhang[a], Robert S. Marks[c], Serge Cosnier[d], Dan Shan[a]*

[a] *School of Environmental and Biological Engineering, Nanjing University of Science and Technology, Nanjing 210094, China*

[b] *Department of Clinical Laboratory, Zhongda Hospital, Southeast University School of Medicine, Nanjing, 210009, Jiangsu, China*

[c] *Department of Biotechnology Engineering, Ben-Gurion University of the Negev, Beer-Sheva, Israel*

[d] *University of Grenoble Alpes-CNRS, DCM UMR 5250, F-38000 Grenoble, France*

*** Corresponding to:**

Prof. Dan Shan

School of Environmental and Biological Engineering,

Nanjing University of Science and Technology,

Nanjing, Jiangsu, 210094, China.

Tel. +86(25) 84303107;

E-mail: danshan@njust.edu.cn

Abstract:

Metal-organic frameworks (MOFs) act as versatile coordinators for the subsequent synthesis of high-performance electrochemical catalysts by providing dispersed metal-ion distribution, initial coordination condition, and modular dopant atom ratios, etc. In this work, a copper-based crystalline MOF *trans*-[$Cu(NO_3)_2(Him)_4$] was synthesized as a novel precursor of a carbon-based electrochemical valence-alternating NC@Cu_xO catalyst. Through simple temperature modulation of the pyrolysis procedure, the gradual transformation towards highly-active catalytic nanocomposite was characterized and investigated to ascertain the signal enhancing mechanism during H_2O_2 detection. Owing to its proprietary structure and ensuing electrochemical reduction activity, a proof-of-principle sensor using NC@Cu_xO as transducer was able to provide an amplified sensitivity of 2330 $\mu A\ mM^{-1}\ cm^{-2}$. In addition, its facile one-vessel preparation and the intrinsic non-enzymatic nature suggests a wide range of potential applications in medical settings.

Keywords:

Metal-organic framework derivate, Non-enzyme catalyst, Electrochemical biosensor, Fenton-like signal amplification, One-pot synthesis

The electrochemically active material, or rather the transducer, plays an imperative role in the construction of an electrochemical biosensor [1]. Its intrinsic properties, such as active center density, electron transfer ability, as well as, internal structure and external morphology, set the fundamental performance of the derived sensing systems or devices [2-4]. Use of metal-organic frameworks (MOFs) as self-sacrificed precursors [5, 6] provides invaluable properties, such as: 1) tunable initial coordination environment and heteroatom doping, that can be easily achieved through the selection of multitudinous ligand molecules; 2) atomic migration process can be accessed and manually paused to obtain a series of products with diverse composite configurations, including metal centers at different valence states or more precisely the nuanced electronic regulation states, or carbon substrates with various interconnecting degrees or doping ratios, and active catalysis clusters with distinguished diameters; 3) porous characteristics can be inherited, thus allowing high-throughput mass diffusion and interfacial contact [7, 8]. Already, some state-of-the-art single atom catalysts (SACs) with satisfactory performance have been synthesized using MOFs as starting templates [9, 10].

Copper-based MOFs or derived nanomaterials have drawn conspicuous attention due to their specific enzyme-like activities, reasonable cost efficiency and robust stability [11-13]. According to the aforementioned advantages, these copper-based enzyme mimics have been well accepted as signal transducers to construct sensitive biosensor systems [14]. Copper species, no matter in

forms of elementary clusters [15, 16], compound nanoparticles [17] or even secondary coordination units [18], show prominent redox activity, with or without, extra potential energy from the external circuit. In some latest articles, more complex copper-based transducer materials with excellent and versatile capabilities were synthesized from MOFs-contained composite precursors, e.g. with several 2D materials like graphene, C_3N_4 or MXene [19]. All these treasures figure out an efficient clue of massively converting homogeneous structural units inside the MOF crystal into highly disperse nano-catalysts decorated upon a simultaneously generated substrate, and meanwhile investigate the transiting procedure of some certain catalysis activity to the other [20].

In the present communication, we designed the synthesis of a crystalline MOF-derived Cu_xO composite catalyst, serving as an electrochemical peroxidase mimic. Inspired by the coordination structure of copper catalysts, both the ligand atoms and the central metal valence state of the catalysis unit were modulated simply using a short period of differential thermal treatment. Thanks to the uniform texture of the crystalline precursor, the generation process of a well-tuned transducer material was monitored and sought. An electrochemical Fenton-like signal enhancing mechanism was herein discussed, in view of the derived prototype biosensor and its corresponding interfacial reactions (Fig. 1A). We expect that this novel and concise transducer material will provide proprietary engineering insights in providing

improved biosensor devices suitable for commercialization [21, 22].

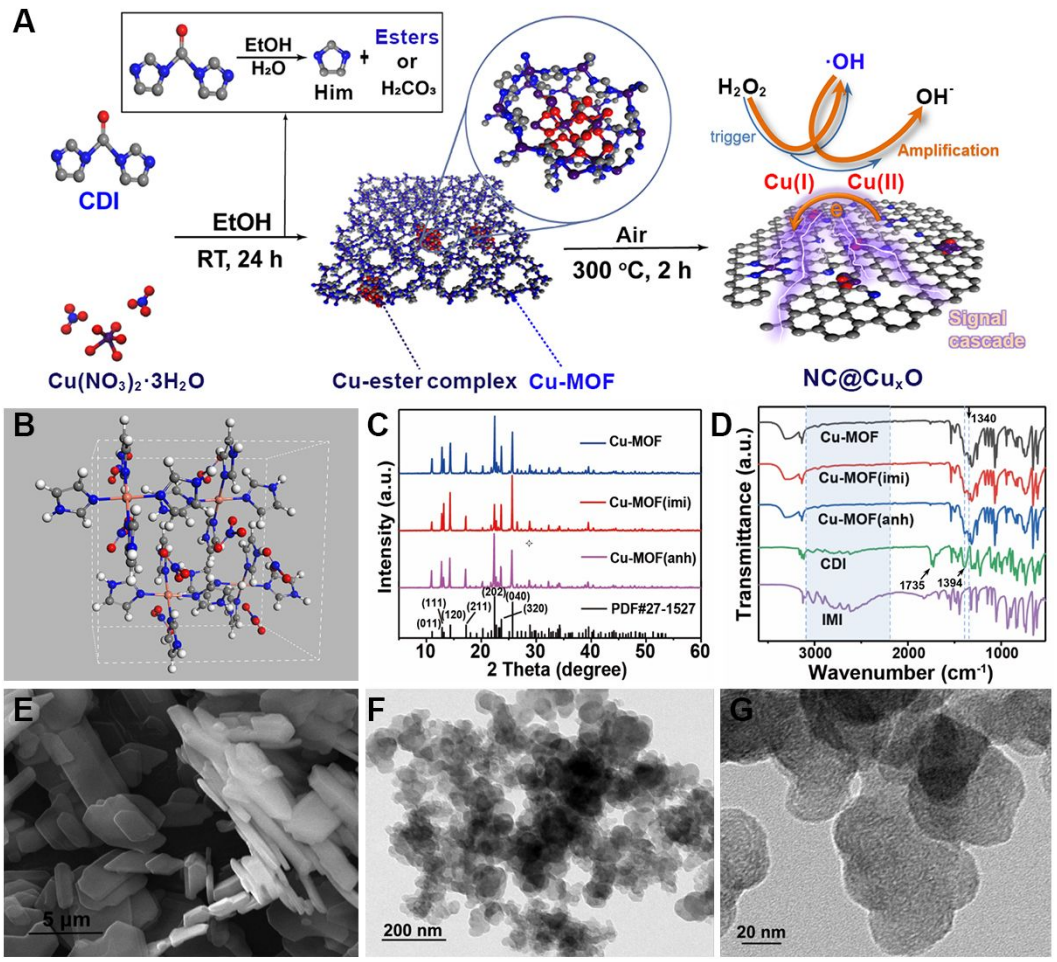

Fig. 1. Stepwise modulation from crystalline MOF precursor to active electrochemical transducer. **(A)** Schematic overview of the preparation and signal amplification mechanism of the composite transducer material NC@Cu_xO. **(B)** Crystal structure diagram of the MOF precursor *trans*-[$Cu(NO_3)_2(Him)_4$]. **(C)** Three comparative routes to prepare MOF precursors with distinguished preferential crystallographic orientation and lattice shrinkage or bulge. **(D)** FT-IR spectra of the obtained crystalline precursors with arrows and blue dashed lines or region indicating critical changes of the transmittance peak. **(E)** SEM image of the board-like precursor cystals. **(F** and **G)** TEM images of the layered transducer material NC@Cu_xO after a short period of pyrolysis under air atmosphere.

To ascertain that copper atoms were highly dispersed at the initial precursor stage, powder X-ray diffraction (PXRD) was performed immediately after lyophilization (Supplementary methods). All of the main peaks have been indexed as a well-defined orthorhombic phase of *trans*-[$Cu(NO_3)_2(Him)_4$]

crystal (PDF 27-1527) [23], indicating that the copper ions were strictly hexa-coordinated by four nitrogen atoms (from imidazole) and two oxygen atoms (belonging to the nitrate ions) (Fig. 1B). The specific crystal herein was obtained according to the following procedures: N,N'-carbonyldiimidazole (CDI) underwent decomposition in some polar solvents like ethanol, thus, releasing free imidazole (Him) molecules as well as di-esters of carbonic acid or imidazole-N-carboxylic esters, as shown in *eq.1*. Whereas, in the presence of lattice water, CDI was possible to be hydrolyzed into carbonate ions (*eq.2*) which would further react with copper ions and generate stable basic modalities [24].

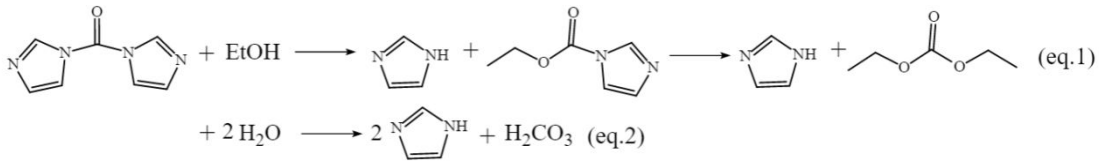

In order to know the priority of the aforementioned possible reaction routes, two contrast synthesis strategies were introduced. In detail, anhydrous copper nitrate with CDI and $CuNO_3 \cdot 3H_2O$ with imidazole were each examined under the same ethanol-solvent condition and compared in terms of their respective diffraction peaks which almost kept the same with a slight peak shift of about 10^{-2} degrees, implying lattice shrinkage and bulge of these copper-imidazole frameworks due to the differences in accessory products (Fig. 1C and Fig. S1) [25]. Interestingly, the preferential crystallographic orientations echoed by the diffraction peak intensities, however, were significantly different between the

two groups. From the Fourier transform infrared spectrometer (FT-IR) spectra, it is clear that these Cu-MOFs acquired through different formulas maintained perfectly identical chemical bonds. The transmittance peak variations from the ligand monomers suggested probable reaction routes and the inner connections of MOFs, detailed as follows: 1) the vanishing of carbonyl stretching vibration at ~1735 cm^{-1}, as well as the strong broad band from 2200 to 3100 cm^{-1}, respectively indicated the decomposition of CDI, and the following coordination reaction of derived imidazole with copper ion which accompanied the collapse of N–H···N hydrogen bonds; and 2) the strong vibration peak at 1394 cm^{-1} that can be assigned to the amide C–N of CDI red-shifted to 1340 cm^{-1} as a result of the formation of ester C–O bonds in all MOF samples (Fig. 1D and Fig. S2) [26]. These results imply that regardless of the presence of lattice water, CDI reacts with ethanol thereby generating ester species.

The bluish violet Cu-MOF powder exhibited tabular hexagon-like morphology with a thickness of hundreds of nanometers in scanning electron microscope (SEM) images (Fig. 1E). After the pyrolysis process under air atmosphere, the resulting NC@Cu_xO catalyst, showed an obviously decreased plane size down to 10-nm scale, according to the transmission electron microscope (TEM) results (Fig. 1F and 1G). Furthermore, the absence of aggregated nanoparticles suggested highly dispersed catalytic sites. To further understand the transformation from a Cu-MOF precursor to a

copper-based catalyst and its accompanying H_2O_2 reduction properties, thermogravimetric-differential scanning calorimetry (TG-DSC) analysis was conducted at a 5 ℃ min^{-1} heating rate (Fig. 2B). A sharp weight loss was noticed from 200 to 240 ℃, accompanied with a clear exothermic peak at 226 ℃. Thereafter, three representative temperature points (200, 300 and 400 ℃) were set with their corresponding products named NC@Cu_xO-L, NC@Cu_xO and NC@Cu_xO-H respectively.

When the Cu-MOF precursor was heated at 200 ℃ for 2 hours, the obtained NC@Cu_xO-L still preserved the typical lattice characteristics of *trans*-[$Cu(NO_3)_2(Him)_4$], and its weight loss can be attributed to the desorption of solvent molecules and the decomposition of thermolabile esters. With a further rise in temperature, broad peaks of graphite and copper oxide appeared in the NC@Cu_xO PXRD spectrum (Fig. 2A). By substituting the measured value of full width at half maximum (FWHM) into the Scherrer equation, the crystallite size of the newly formed copper oxide was calculated to be several nanometers, which was in accordance with the lack of gathered clusters in the TEM image [27]. *Via* calcination at 400 ℃, the derived NC@Cu_xO-H showed striking peaks identical to that of CuO, owing to the deep substitution of oxygen for the initial coordinated nitrogen through atomic transfer.

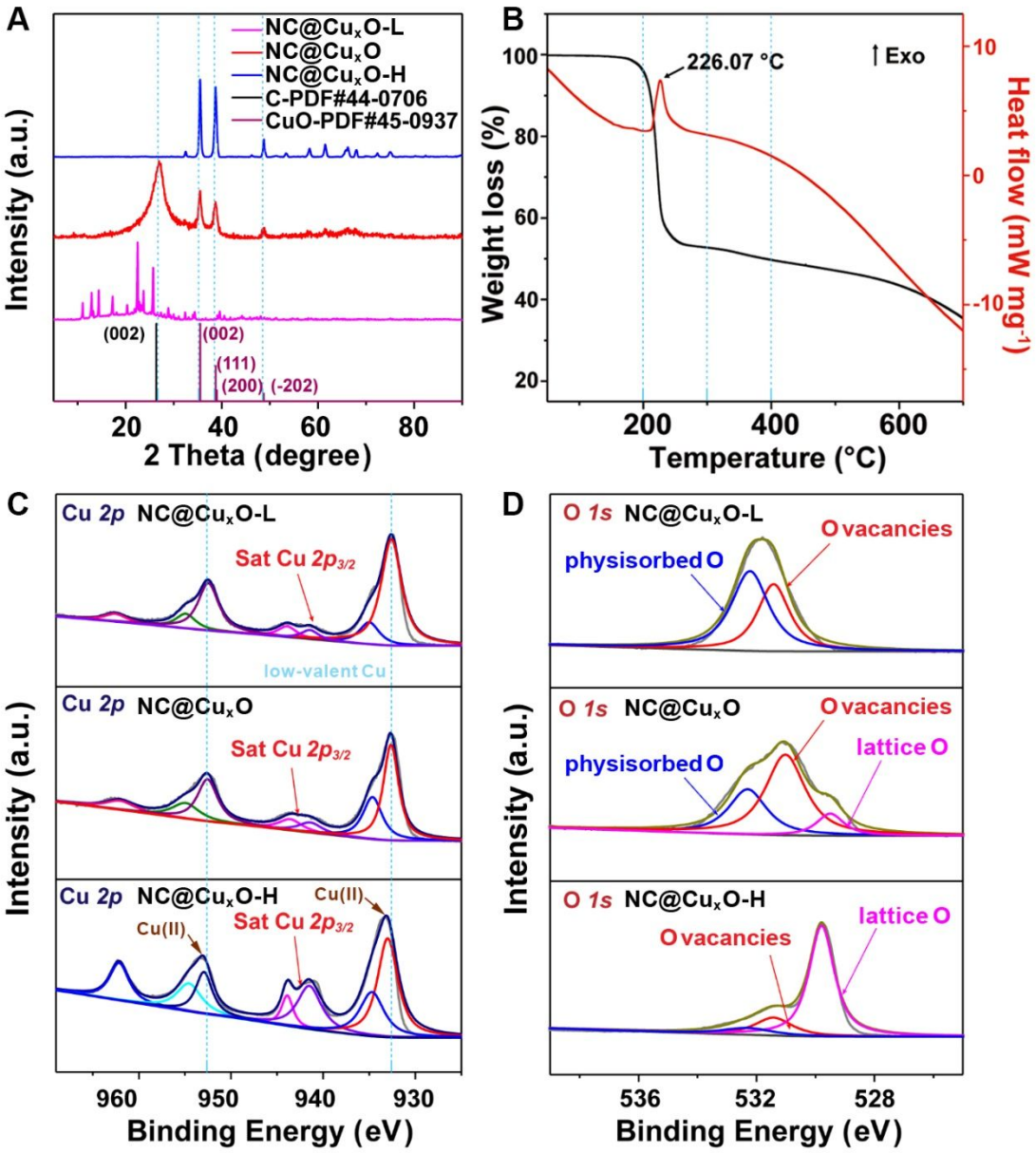

Fig. 2. Temperature modulation of the valence state of the central metal as well as the neighboring ligand atoms and vacancies. **(A)** XRD spectra of the pyrolyzed samples under different heat-treatment temperature. **(B)** TG-DSC curves of the self-sacrifice MOF precursor in air atmosphere with the heating rate of 5 ℃ min^{-1}. High-resolution XPS spectra of Cu 2p **(C)** and O 1s **(D)** orbitals of the under-heated NC@Cu_xO-L, experimental NC@Cu_xO and over-heated NC@Cu_xO-H samples.

A mutually corroborating result was obtained by investigating the chemical state alternations of atoms. In both NC@Cu_xO-L and NC@Cu_xO samples, the high-resolution X-ray photoelectron spectroscopy (XPS) spectra of Cu 2p orbitals displayed relatively weaker satellite peaks and slightly lower binding

energies of both the $2p_{1/2}$ and $2p_{3/2}$ orbitals than that of NC@Cu_xO-H (Fig. 2C). Due to the existence of CuO nanocrystalline in NC@Cu_xO, we surmised that these features ought to be attributed to the abundant intermediate low-valent Cu(I) rather than Cu(II) of coordinated state or compound state [28]. Taking O 1s spectra into consideration, on the other dimension, the gradual shift of the predominant sub-peaks from 532.2 to 529.7 eV can help determine the exact components of the aforementioned NC@Cu_xO catalysts. In detail, NC@Cu_xO-L displayed Cu-MOF-like characteristics with respect to crystal structure, and the chemical state of organic oxygen assigned as incompletely decomposed esters. NC@Cu_xO-H, at the other extreme, exhibited canonical CuO properties with a standard XRD pattern and typical XPS spectrum features, such as the intensive satellite peaks of Cu 2p and the nearly complete conversion to lattice oxygen which belongs to the metal-oxide compounds (Fig. 2D).

The aforementioned under- or over- heating treatments exhibit variance in the resulting functional ingredient of the composite catalyst NC@Cu_xO. On one hand, the crystalline framework collapsed and recombined as a N-doped carbon substrate. The copper atoms, on the other hand, were gradually aggregated and oxidized into nanoscale CuO nanoparticles, while preserving an overall amorphous state with abundant oxygen vacancies (Fig. 2D) [29]. Therefore, the uniformly dispersed catalytic centers of reductive copper oxide in NC@Cu_xO determined their high reaction activity towards oxidizing

substances. Simultaneously, the internal structural porosity is substantially retained which guarantees sufficient mass transfer during the catalyzing procedures (Fig. S3 and S4). The Cu-MOF precursor's periodic atom distributions and definite melting point enable the investigation of some critical catalyst-evolving processes, such as metal migration and oxygen transfer, by simply modulating temperature.

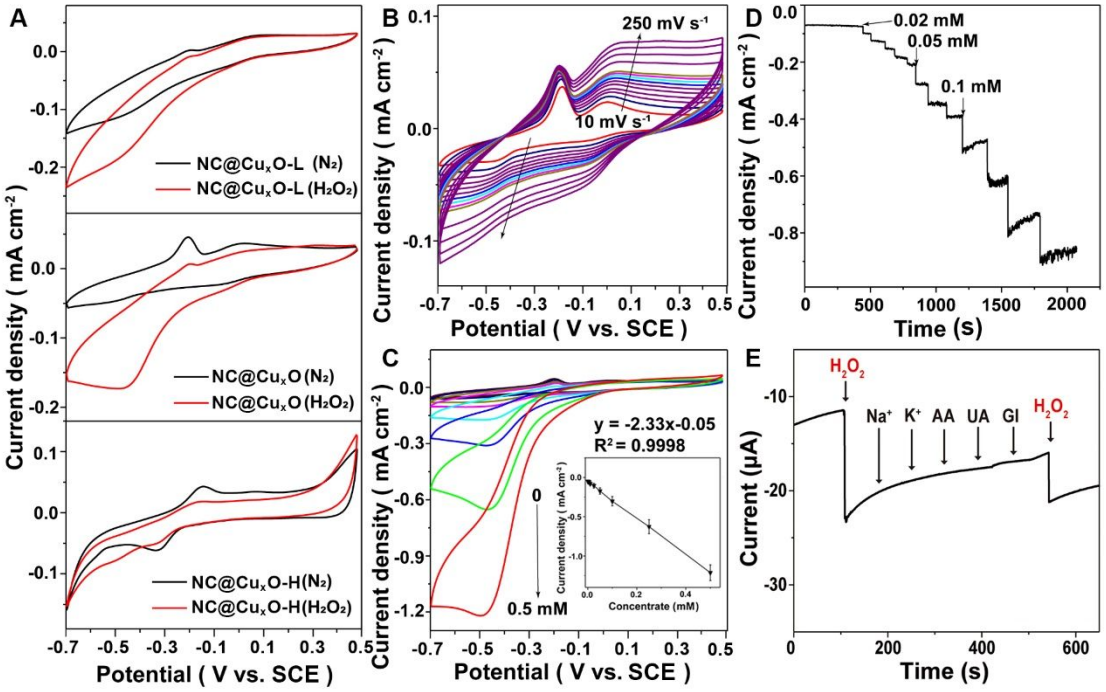

Fig. 3. Electrochemical catalysis behavior investigation of the transducer material to support sensitive sensing of H_2O_2 concentration. **(A)** Electrochemical redox characteristics of the MOF-residual dominant (NC@Cu_xO-L, top), O-vacancy abundant (NC@Cu_xO, middle) and deeply oxidized (NC@Cu_xO-H, bottom) samples as transducers in the absence and presence of 0.05 mM H_2O_2. **(B)** Cyclic voltammograms of NC@Cu_xO electrode at different scan rates from 10 to 250 mV s^{-1} in condition of saturated nitrogen without H_2O_2. **(C)** Cyclic voltammogram of NC@Cu_xO electrode in response to H_2O_2 concentrations of 0 to 0.5 mM with an insert exhibiting the linear fitting of the reductive peak-current density values. **(D)** Chronoamperometric responses of NC@Cu_xO to stepwise addition of H_2O_2 at -0.5 V (vs. SCE). **(E)** Selectivity test of the biosensor against some common interferences in body fluid, including 1 mM Na^+, K^+, ascorbic acid, uric acid and glucose.

Based on the characteristics of the NC@Cu_xO catalyst species, their respective electrochemical behaviors were further examined using cyclic

voltammetry (CV) (Fig. 3A). In the absence of H_2O_2, the lower-heated sample showed inconspicuous redox peaks, implying an inert electron transfer ability of the Cu-N coordinate-bond dominated MOF material. In contrast, the 400 ℃ pyrolyzed product exhibited both obvious redox peaks (Cu^{I}/Cu^{II}, E_p= -0.34 and -0.15 V) due to the formation of conductive carbon substrates. In regard to the NC@Cu_xO, its undiscovered reduction peak at this particular potential window indicated that copper existed in a low valence state in Cu_xO and the electrochemically oxidized copper ions would then be released into the liquid phase, resulting in an irreversible procedure. When the solution contained 0.05 mM H_2O_2, a strong reduction peak appeared around -0.45 V, significantly deviating from the CV curve without adding H_2O_2. It is worth noting that the oxidization peak, in the meanwhile, became quite indistinct especially when the H_2O_2 concentration increased. This result implied that reductive copper in NC@Cu_xO preferred to react with the oxidizing substances derived from H_2O_2 decomposition, prior to being electrochemically oxidized at the anode (*eq.3*).

The emphasis in sensitive H_2O_2 detection lays on enhanced signal transduction or an amplified feedback. Therefore, the catalysis mechanism and its signal conversion process was studied first. The NC@Cu_xO modified glassy carbon electrode (GCE) was tested by cyclic voltammetry at different scan rates in 0.1 M PBS and 0.3 M KCl solution (Fig. 3B). With increasing scan rate from 10 to 250 mV s^{-1}, both of the anodic and cathodic peak currents were measured as linear with the square root of the scan rate (Fig.

S5), indicating characteristic diffusion-controlled electrochemical redox behaviors [30] from which we inferred a Fenton-induced enhancing mechanism:

Trigger: $NC@Cu_xO_{red,Cu(I)} + H_2O_2 \rightarrow NC@Cu_xO_{ox,Cu(II)} + \cdot OH + OH^-$ (eq.3)

Amplification: $NC@Cu_xO_{red,Cu(I)} + \cdot OH \rightarrow NC@Cu_xO_{ox,Cu(II)} + OH^-$ (eq.4)

Transduction and Reset: $NC@Cu_xO_{ox,Cu(II)} + e^- \rightarrow NC@Cu_xO_{red,Cu(I)}$ (eq.5)

The highly dispersed Cu(I) catalysis centers of Cu_xO efficiently accelerated the decomposition of H_2O_2, while releasing an equivalent amount of ·OH radicals. Thereafter, increased reductive copper sites would be oxidized through rapid radical reactions. At the reduction potential, the newly generated Cu(II) would then get reduced by capturing the electrons from the outer circuit. More importantly, the electrochemical procedures at the electrodes were shown to be rapid, which meant this redox cycle (*eq.3-5*) would continuously proceed until the diffusion limit and simultaneously provide amplified current response [31]. In addition, this catalytic process relied on not only the valence state of copper centers, but also the structural configuration of ligand atoms and defects, which can be supposed from the poor activity of both the $NC@Cu_xO$-L and $NC@Cu_xO$-H samples.

By adding H_2O_2 solutions of differing concentrations (Fig. 3C), the current intensity of the reduction peak at -0.45 V was identified as a linear coefficient of the concentration, with a corresponding linear equation: j (mA cm^{-2}) =

-2.33C (mM) - 0.05 (R^2=0.9998), ranging from 10 μM to 0.5 mM. The limit of detection for the NC@Cu_xO sensor, (LOD= $3\sigma/S_d$, where σ represents the standard deviation of the current density value measured in blank solution, and S_d stands for the slope of linear regression calibration line), reached 6.67 nM. Fig. 3D shows the amperometric response towards concentrated H_2O_2 solutions. The cathodic current rapidly achieved steady states and increased in pace with the addition of H_2O_2. The selectivity and stability of this proof-of-principle biosensor were also evaluated as these two important parameters could reflect whether an artificial catalyst could mimic or even surpass natural enzymes in practical use. From Fig. 3E, we can conclude that NC@Cu_xO has good selectivity towards H_2O_2. The i-t curve in Fig. S6 exhibited the stability of this electrochemical sensor for long-term continuous detection. After dropping in 1 mM H_2O_2 solution, the output current could keep steady for more than 1 h, indicating that the NC@Cu_xO nanocomposite did not leach out from the electrode during multiple cycles of electrochemical redox process, while maintaining high catalytic activity. By simply modulating the thermal redox condition of a well-characterized crystalline MOF precursor, both the chemical valence and coordination environment of the central metal were adjusted to render a transducer enhanced signal feedback. In comparison with previous studies which introduced other functional materials or not, this NC@Cu_xO electrode offers a highly competitive sensitivity, as well as other decent performances (Table 1).

Table 1. Comparison of copper-based electrochemical H_2O_2 transducer materials on catalysis mechanism and sensitivity performance.

Transducer material	Active-center type	Redox potential (V)	Additional materials	Sensitivity ($\mu A\ mM^{-1}\ cm^{-2}$)	LOD (μM)	References
CuO nanoflowers	monoclinic CuO	-0.4 (vs. Ag/AgCl)	n.a.	956.69	0.85	[32]
Cu_2O nanopaticles	~100 nm size with (111) facets	-0.42 (vs. Ag/AgCl)	n.a.	28.0	0.2	[33]
3DIO Au/NiO@CuO	Ni^{3+} species	0.5 (vs. Ag/AgCl)	CuO skeleton & AuNPs	650.2	0.0037	[34]
CuNPs@Y-1,4-NDC-MOF/ERGO	CuNPs supported by ERGO	-0.2 (vs. SCE)	Y-1,4-NDC-MOF & ERGO	8.8	0.43	[35]
Cu_2O-rGO-P	cubic Cu_2O	-0.4 (vs. Ag/AgCl)	rGO paper	77*	3.78	[36]
NCNT MOF CoCu	Co(0) & Cu(0)	0.5 (vs. Ag/AgCl)	Co(0)	639.5	0.206	[37]
Cu-Mo_2C/C	Synergic Mo_2C with Cu(0)	-0.4 (vs. SCE)	hexagonal β-Mo_2C	392.7	0.04	[38]
NC@Cu_xO	**Amorphous Cu_xO with oxygen vacancies**	**-0.45 (vs. SCE)**	**n.a.**	**2330**	**0.00667**	**This work**

* estimated from the offered linear regression curve.

We presented, herein, a sensitive H_2O_2 sensor constructed with a tailored amorphous Cu_xO composite catalyst. The corresponding mechanism of enhanced signal transduction were stepwise investigated from the precursor conformation, to its catalytic evolution, up to a final amplified electron cascades. With the initial copper-nitrogen square domains converting into low-valent amorphous copper oxide catalytic centers, the resulting current remarkably increased due to its synergistic enhancement, contributed by both rapid radical and electrochemical reactions. Moreover, the structural property of specific neighboring ligand-atom configuration was proven to be a factor as predominant as the valence state of central metals. From the perspective of material, catalysis and the final sensing application, the way to design and

modulate a proper copper-based transducer was comprehensively explored. We envision that our work would hold the prospect for accurate bio-analyte quantitation and promote the mainstreaming of precision diagnosis and medicine.

Acknowledgements

The authors greatly acknowledge the financial support from National Natural Science Foundation of China (Grant No. 62001224), Natural Science Foundation of Jiangsu Province (Grant No. BK20190457), "Overseas Academic Partnership Program" of Nanjing University of Technology (2019), and Sino-French international research network "New nanostructured materials and biomaterials for renewable electrical energy sources"

1. Zhao, S.; Zang, G.; Zhang, Y.; Liu, H.; Wang, N.; Cai, S.; Durkan, C.; Xie, G.; Wang, G., Recent advances of electrochemical sensors for detecting and monitoring ROS/RNS. *Biosens. Bioelectron.* **2021,** *179*, 113052.

2. Sehit, E.; Altintas, Z., Significance of nanomaterials in electrochemical glucose sensors: An updated review (2016-2020). *Biosens. Bioelectron.* **2020,** *159*, 112165.

3. Lu, S.-M.; Peng, Y.-Y.; Ying, Y.-L.; Long, Y.-T., Electrochemical Sensing at a Confined Space. *Anal. Chem.* **2020,** *92* (8), 5621-5644.

4. Lawal, A. T., Graphene-based nano composites and their applications. A review. *Biosens. Bioelectron.* **2019,** *141*, 111384.

5. Ji, D.; Zhou, H.; Tong, Y.; Wang, J.; Zhu, M.; Chen, T.; Yuan, A., Facile

fabrication of MOF-derived octahedral CuO wrapped 3D graphene network as binder-free anode for high performance lithium-ion batteries. *Chem. Eng. J.* **2017,** *313*, 1623-1632.

6. Wang, H.-F.; Chen, L.; Pang, H.; Kaskel, S.; Xu, Q., MOF-derived electrocatalysts for oxygen reduction, oxygen evolution and hydrogen evolution reactions. *Chem. Soc. Rev.* **2020,** *49* (5), 1414-1448.

7. Bavykina, A.; Kolobov, N.; Khan, I. S.; Bau, J. A.; Ramirez, A.; Gascon, J., Metal-Organic Frameworks in Heterogeneous Catalysis: Recent Progress, New Trends, and Future Perspectives. *Chem. Rev.* **2020,** *120* (16), 8468-8535.

8. Yang, Q.; Xu, Q.; Jiang, H.-L., Metal-organic frameworks meet metal nanoparticles: synergistic effect for enhanced catalysis. *Chem. Soc. Rev.* **2017,** *46* (15), 4774-4808.

9. Sun, T.; Xu, L.; Wang, D.; Li, Y., Metal organic frameworks derived single atom catalysts for electrocatalytic energy conversion. *Nano Res.* **2019,** *12* (9), 2067-2080.

10. Ji, S.; Chen, Y.; Wang, X.; Zhang, Z.; Wang, D.; Li, Y., Chemical Synthesis of Single Atomic Site Catalysts. *Chem. Rev.* **2020,** *120* (21), 11900-11955.

11. Bao, J.; Yang, G.; Yoneyama, Y.; Tsubaki, N., Significant Advances in C1 Catalysis: Highly Efficient Catalysts and Catalytic Reactions. *ACS Catalysis* **2019,** *9* (4), 3026-3053.

12. Wang, R.; Dong, X. Y.; Du, J.; Zhao, J. Y.; Zang, S. Q., MOF-Derived Bifunctional Cu_3P Nanoparticles Coated by a N,P-Codoped Carbon Shell for Hydrogen Evolution and Oxygen Reduction. *Adv. Mater.* **2018,** *30* (6), 29266417.

13. Abdel-Mageed, A. M.; Rungtaweevoranit, B.; Parlinska-Wojtan, M.; Pei, X.; Yaghi, O. M.; Behm, R. J., Highly Active and Stable Single-Atom Cu Catalysts Supported by a Metal-Organic Framework. *J. Am. Chem. Soc.* **2019,** *141* (13), 5201-5210.

14. Xiangyu, L.; Shanshan, G.; Han, L.; Luodan, Y.; Yunhu, H.; Piao, Z.; Weichao, B.; Heliang, Y.; Yu, C.; Jianlin, S., Bioinspired Copper Single-Atom Catalysts for Tumor Parallel Catalytic Therapy. *Adv. Mater.* **2020,** *32* (36), 2002246.

15. Subarna, M.; Dipankar, B.; Sikta, C.; Sarita, K.; Amitava, P., Copper Nanocluster (Cu_{23} NC)-Based Biomimetic System with Peroxidase Activity. *ACS Sustainable Chem. Eng.* **2020,** *8* (49), 18335-18344.

16. Mei-Chen, P.; Yan-Mei, L.; Ya-Qin, C.; Ruo, Y.; Ying, Z., In Situ Controllable Generation of Copper Nanoclusters Confined in a Poly-l-Cysteine Porous Film with Enhanced Electrochemiluminescence for Alkaline Phosphatase Detection. *Anal. Chem.* **2020,** *92* (19), 13581-13587.

17. Wang, W.; Zhang, Y.; Zhang, J.; Li, G.; Leng, D.; Gao, Y.; Gao, J.; Lu, H.; Li, X., Metal-organic framework-derived Cu_2O-CuO octahedrons for sensitive and selective detection of ppb-level NO_2 at room temperature. *Sens. Actuators, B* **2021,** *328*, 129045.

18. Wang, B.; Luo, Y.; Gao, L.; Liu, B.; Duan, G., High-performance field-effect transistor glucose biosensors based on bimetallic Ni/Cu metal-organic frameworks. *Biosens. Bioelectron.* **2021,** *171*, 112736.

19. Wang, D.; Zhang, D.; Yang, Y.; Mi, Q.; Zhang, J.; Yu, L., Multifunctional Latex/Polytetrafluoroethylene-Based Triboelectric Nanogenerator for Self-Powered Organ-like MXene/Metal-Organic Framework-Derived CuO Nanohybrid Ammonia Sensor. *ACS Nano* **2021,** *15* (2), 2911-2919.

20. Chen, Y.-Z.; Zhang, R.; Jiao, L.; Jiang, H.-L., Metal-organic framework-derived porous materials for catalysis. *Coord. Chem. Rev.* **2018,** *362*, 1-23.

21. Goud, K. Y.; Reddy, K. K.; Khorshed, A.; Kumar, V. S.; Mishra, R. K.; Oraby, M.; Ibrahim, A. H.; Kim, H.; Gobi, K. V., Electrochemical diagnostics of infectious viral diseases: Trends and challenges. *Biosens. Bioelectron.* **2021,** *180*, 113112.

22. Cesewski, E.; Johnson, B. N., Electrochemical biosensors for pathogen detection. *Biosens. Bioelectron.* **2020,** *159*, 112214.

23. Stamatatos, T. C.; Perlepes, S. P.; Raptopoulou, C. P.; Terzis, A.; Patrickios, C. S.; Tasiopoulos, A. J.; Boudalis, A. K., Alcoholysis/hydrolysis of 1,1 '-carbonyldiimidazole as a means of preparing unprecedented, imidazole-containing one-dimensional coordination polymers of copper(II). *Dalton Trans.* **2009,** (17), 3354-3362.

24. Staab, H. A., New Methods of Preparative Organic Chmistry IV. Syntheses Using Heterocyclic Amides (Azolides). *Angew. Chem., Int. Ed.* **1962,** *1* (7), 351-367.

25. Yao, M.-S.; Zheng, J.-J.; Wu, A.-Q.; Xu, G.; Nagarkar, S. S.; Zhang, G.; Tsujimoto, M.; Sakaki, S.; Horike, S.; Otake, K.; Kitagawa, S., A Dual-Ligand Porous Coordination Polymer Chemiresistor with Modulated Conductivity and Porosity. *Angew. Chem., Int. Ed.* **2020,** *59* (1), 172-176.

26. Hadrich, A.; Dulong, V.; Rihouey, C.; Labat, B.; Picton, L.; Cerf, D. L., Biomimetic hydrogel by enzymatic crosslinking of pullulan grafted with ferulic acid. *Carbohydr. Polym.* **2020,** *250*, 116967.

27. Abdullah, F. H.; Abu Bakar, N. H. H.; Abu Bakar, M., Comparative study of chemically synthesized and low temperature bio-inspired Musa acuminata peel extract mediated zinc oxide nanoparticles for enhanced visible-photocatalytic degradation of organic contaminants in wastewater treatment. *J. Hazard. Mater.* **2021,** *406*, 124779.

28. Yang, P.-P.; Zhang, X.-L.; Gao, F.-Y.; Zheng, Y.-R.; Niu, Z.-Z.; Yu, X.; Liu, R.; Wu, Z.-Z.; Qin, S.; Chi, L.-P.; Duan, Y.; Ma, T.; Zheng, X.-S.; Zhu, J.-F.; Wang, H.-J.; Gao, M.-R.; Yu, S.-H., Protecting Copper Oxidation State via Intermediate Confinement for Selective CO_2 Electroreduction to C2+ Fuels. *J. Am. Chem. Soc.* **2020,** *142* (13), 6400-6408.

29. Xiao, Z.; Huang, Y.-C.; Dong, C.-L.; Xie, C.; Liu, Z.; Du, S.; Chen, W.; Yan, D.; Tao, L.; Shu, Z.; Zhang, G.; Duan, H.; Wang, Y.; Zou, Y.; Chen, R.; Wang, S., Operando Identification of the Dynamic Behavior of Oxygen Vacancy-Rich Co_3O_4 for Oxygen Evolution Reaction. *J. Am. Chem. Soc.* **2020,** *142* (28), 12087-12095.

30. Fang, Y.; Luan, D.; Chen, Y.; Gao, S.; Lou, X. W., Rationally Designed Three-Layered Cu_2S@Carbon@MoS_2 Hierarchical Nanoboxes for Efficient Sodium Storage. *Angew. Chem., Int. Ed.* **2020,** *59* (18), 7178-7183.

31. Savéant, J.-M., Molecular Catalysis of Electrochemical Reactions. Cyclic Voltammetry of Systems Approaching Reversibility. *ACS Catalysis* **2018,** *8* (8), 7608-7611.

32. Ni, Y.; Sun, Z.; Zeng, Z.; Liu, F.; Qin, J., Hydrothermal fabrication of hierarchical CuO nanoflowers for dual-function amperometric sensing of hydrogen peroxide and glucose. *New J. Chem.* **2019,** *43* (47), 18629-18636.

33. Juang, F.-R.; Chern, W.-C., Controlled Synthesis of Cuprous Oxide Nanoparticles with Different Morphologies for Nonenzymatic Hydrogen Peroxide Sensing Applications. *J. Electrochem. Soc.* **2019,** *166* (4), B200-B204.

34. Zhou, X.; Xu, L.; Lv, J.; Yang, S.; Zhu, S.; Chen, X.; Sun, X.; Dong, B.; Bai, X.; Lu, G.; Song, H., Au anchored three-dimensional macroporous NiO@CuO inverse opals

411 for in-situ sensing of hydrogen peroxide secretion from living cells. *Sens. Actuators, B* **2019,**
412 *297*, 126729.
413 35. Li, C.; Wu, R.; Zou, J.; Zhang, T.; Zhang, S.; Zhang, Z.; Hu, X.; Yan, Y.; Ling,
414 X., MNPs@anionic MOFs/ERGO with the size selectivity for the electrochemical
415 determination of H_2O_2 released from living cells. *Biosens. Bioelectron.* **2018,** *116*, 81-88.
416 36. Cheng, C.; Zhang, C.; Gao, X.; Zhuang, Z.; Du, C.; Chen, W., 3D Network and 2D
417 Paper of Reduced Graphene Oxide/Cu_2O Composite for Electrochemical Sensing of
418 Hydrogen Peroxide. *Anal. Chem.* **2018,** *90* (3), 1983-1991.
419 37. Kim, S. E.; Muthurasu, A., Highly Oriented Nitrogen-doped Carbon Nanotube Integrated
420 Bimetallic Cobalt Copper Organic Framework for Non-enzymatic Electrochemical Glucose
421 and Hydrogen Peroxide Sensor. *Electroanalysis* **2021,** *33*, 1-14.
422 38. Li, B.; Liu, L.-H.; Zhang, X.-F.; Gao, Y.; Deng, Z.-P.; Huo, L.-H.; Gao, S.,
423 Echinus-like Cu-Mo_2C/C yolk-shell composites for ultrasensitive detection of hydrogen
424 peroxide. *Electrochim. Acta* **2021,** *373*, 137908.
425